The effects of water vapour on the hot corrosion of gas turbine blade materials at 700 °C

Andrew Potter, Joy Sumner & Nigel Simms

Published online: 28 Mar 2022.

Submit your article to this journal ⬚

View related articles ⬚

View Crossmark data ⬚

The effects of water vapour on the hot corrosion of gas turbine blade materials at 700 °C

Andrew Potter, Joy Sumner and Nigel Simms

Centre for Thermal Energy Systems and Materials, Cranfield University, Cranfield UK

ABSTRACT

Future developments in power generation are likely to require gas turbines to operate in novel combustion environments. The level of water vapour in the turbine's gas stream is one variable that may change as a consequence. This paper explores the effects of water vapour on hot corrosion. The 'deposit recoat' technique was used to evaluate the hot corrosion performance of superalloys PWA 1483 and MarM 509 in atmospheres containing between 0 and 20 vol.% water vapour. Exposures were carried out at 700 °C in atmospheres containing 300 ppm SO_2 for up to 500 hours. The deposit was an 80% Na_2SO_4, 20% K_2SO_4 solution applied with a deposition flux of 1.5 μg/cm^2/h. The findings are compared to similar exposures with 3.6 ppm SO_2.

Increasing levels of water vapour were observed to reduce sound metal loss in atmospheres containing 300 ppm SO_2 while increasing sound metal loss in atmospheres containing 3.6 ppm SO_2.

Introduction

The majority of the driving force behind the development of future industrial gas turbine technologies aims to achieve two things: increased efficiency of power generation and a reduction in CO_2 gas emissions [1]. To meet these two objectives, gas turbines are likely to be required to operate under novel conditions. These could include higher firing temperatures to achieve greater thermal efficiencies and the combustion of alternative fuels. Hydrogen rich syngas derived from the gasification of solid fuels is a potential form the new fuels may take [2].

The level of water vapour in the gas stream passing through the power turbine section of an industrial gas turbine is one variable influenced by the type of fuel combusted [3]. For example, power turbine environments resulting from the combustion of natural gas have been calculated to contain approximately 10 vol.% water vapour, whereas power turbine environments resulting from the combustion of hydrogen-rich syngas are expected to contain approximately 20 vol.% water vapour [4].

The effect water vapour has on the oxidation of materials typically used in high temperature applications has been investigated by a number of authors [5–8]. Most authors observe increased rates of oxidation for Cr_2O_3 forming alloys in environments containing water vapour. One mechanism explaining this increased rate of oxidation is through the formation of volatile $CrO_2(OH)_3$ and $Cr(OH)_3$ species that may

be subsequently vaporised [6,7]. J. Zurek et al. attributed increased oxidation rates to an observed decrease in the chromia grain size, however these observations were made in a low pO_2 atmosphere [9].

Hot corrosion is an accelerated form of degradation through the amphoteric fluxing of salt species rather than having condensed onto component surfaces [10,11]. Hot corrosion is recognised to occur in two stages: an incubation stage where little metal loss occurs followed by a propagation stage where catastrophic metal loss occurs [12]. The length of the incubation stage is thought to correspond to the breakdown of the protective oxide scale of the afflicted alloy. It is therefore plausible that if water vapour can degrade the protective chromia scale of a chromia forming alloy (either through vaporisation or another method), then it can be postulated that water vapour will increase hot corrosion rates through the shortening of the incubation period.

Previous research has compared hot corrosion in atmospheres generated through the combustion of natural gas and hydrogen-rich syngas [13]. These environments had water vapour contents of 10 and 20 vol.%, respectively, and an SO_x content of 3.6 ppm. The deposit used was 80% Na_2SO_4 20% K_2SO_4 (molar ratio) applied at a flux of 1.5 μg/cm^2/h. Under these conditions, corrosion rates appeared more rapid in the atmosphere containing 20 vol.% with exposures in the 10 vol.% water vapour atmosphere remaining in incubation over the 500 hour
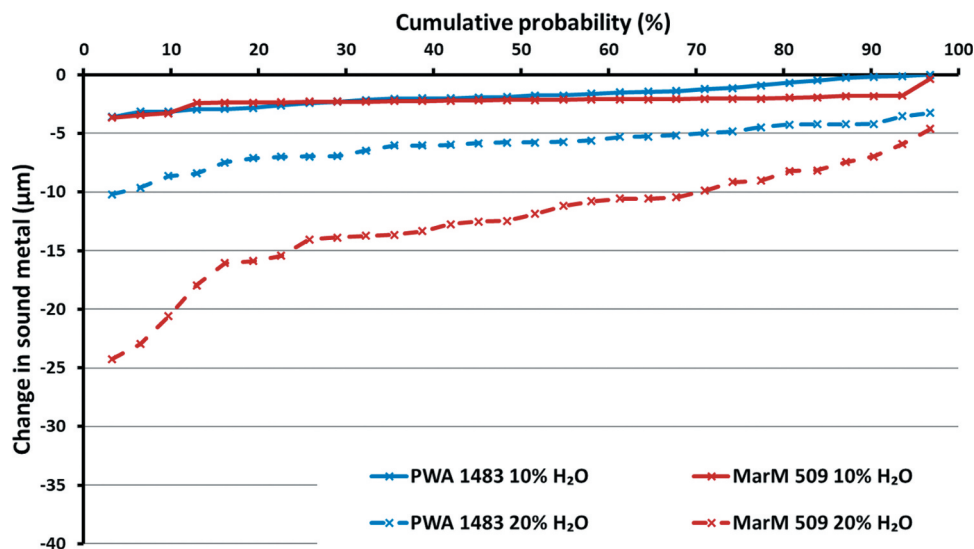
Figure 1. Probability plot of sound metal loss for 500 hour exposures in combustion atmospheres containing 3.6 ppm SO_x with 10 and 20% H_2O at 700 °C in 80/20 $(Na/K)_2SO_4$ deposit applied cyclically with a flux of 1.5 µg/cm^2/h.

test period. The median probability of change in sound metal exceedance plots for these exposures is given in Figure 1.

Methodology

The effects of increasing levels of water vapour on hot corrosion have been investigated using the 'deposit recoat' method. This involves the cyclic high temperature exposure of samples with deposits applied at the start and between each cycle [14].

Exposures were carried out in a vertically aligned tube furnace fitted with a ceramic corrosion vessel (Figure 2), with samples located within the furnace hot zone (±5 °C of target temperature) using a ceramic carousel. The test gas (300 ppm SO_2 in air) was passed through the centre of the carousel to enter the corrosion vessel from the bottom and exit from the top of the furnace. This gas pathway allows time for the SO_2 to reach an equilibrium with SO_3. Water was injected into the gas steam as it passes through the carousel using an independently calibrated peristaltic pump. Three different concentrations of water vapour in the test atmosphere were tested; 0, 10 and 20 vol.%. A deposit of 80% Na_2SO_4 20% K_2SO_4 applied to the samples, heated to approximately 100°C, at a flux of 1.5 µg/cm^2/h using a compressed air fed spray gun. Samples were removed after 50, 100, 200 and 500 hours of exposure.
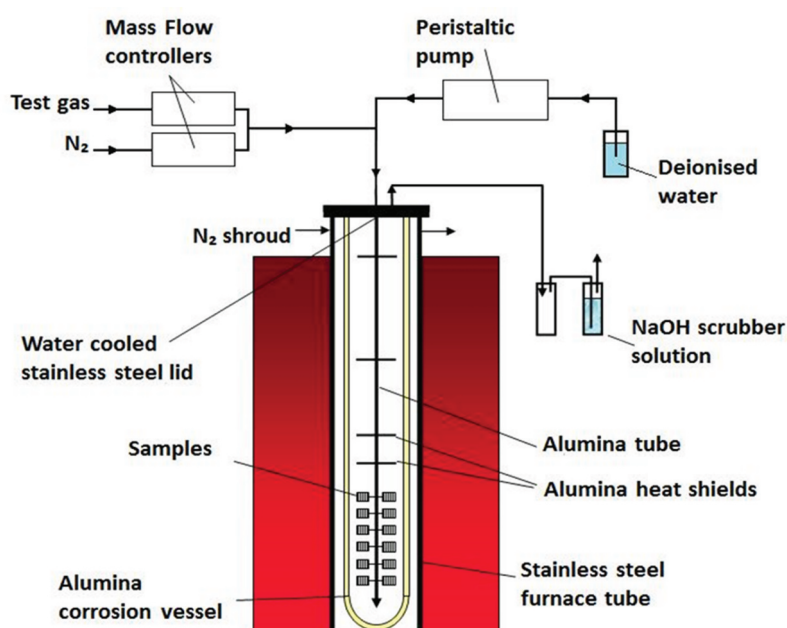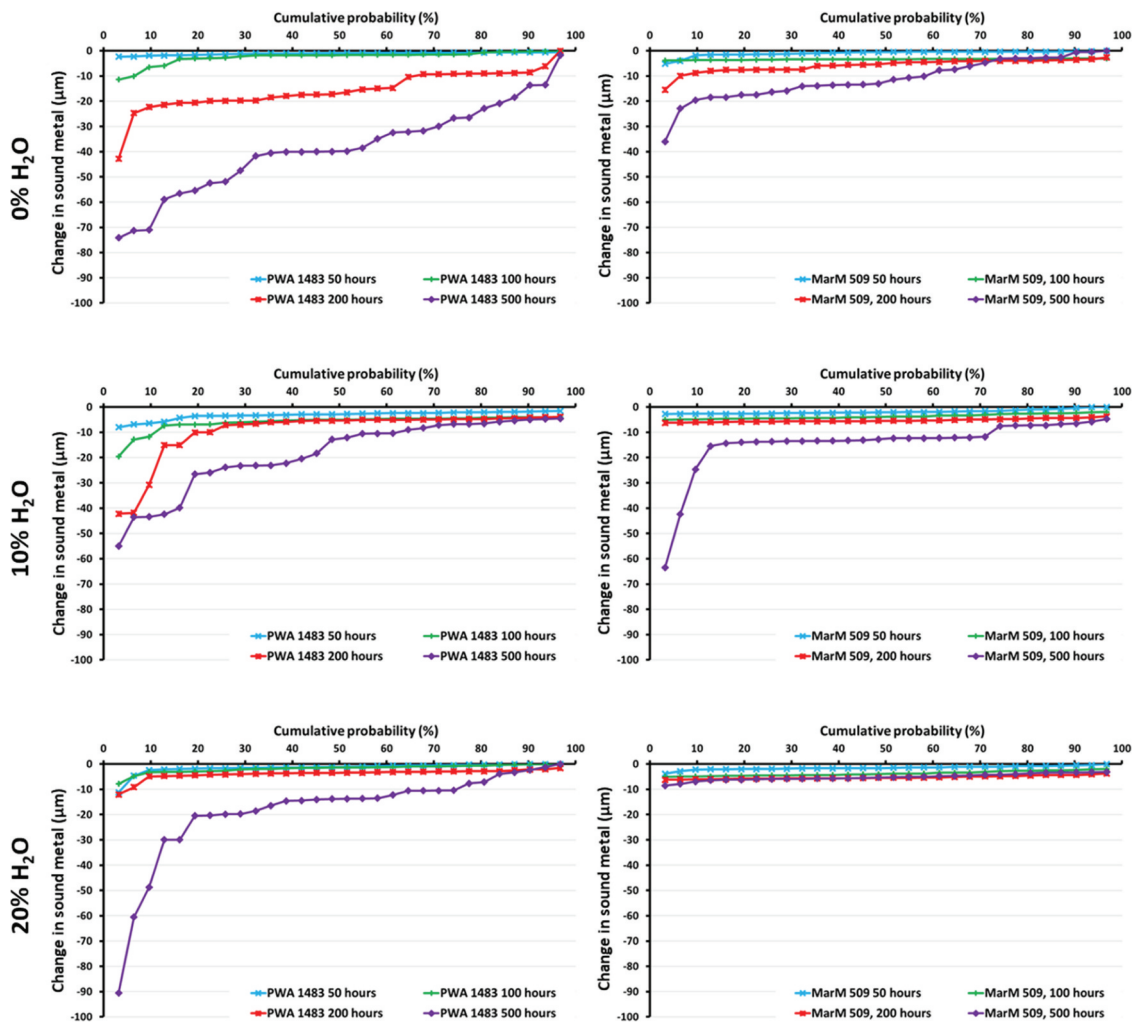

Figure 2. Test furnace apparatus.

Table 1. Nominal alloy elemental compositions.

Alloy	Ni	Co	Cr	Ti	W	Al	Ta	Mo	C	Zr
PWA 1483 (wt.%)	Bal	9	12.2	4.1	3.8	3.6	5	1.9	0.07	...
MarM 509 (wt.%)	10	Bal	23.5	0.2	7	...	3.5	...	0.6	0.5
PWA 1483 (at.%)	Bal	8.9	13.7	5	1.2	7.8	1.6	1.2	0.3	...
MarM 509 (at.%)	10.2	Bal	27.1	0.3	2.3	...	1.2	...	3	0.3

Table 2. Partial pressure (atm) of species present in the considered atmospheres at 700 °C calculated using MT Data thermodynamic modelling software.

	6 % CO_2 8 % O_2 3.6 ppm SO_2 10 % H_2O Balance N_2	1 % CO_2 8 % O_2 3.6 ppm SO_2 20 % H_2O Balance N_2	300 ppm SO_2 Balance air	300 ppm SO_2 10 % H_2O Balance air	300 ppm SO_2 20 % H_2O Balance air
CO_2	6.00E-02	9.67E-03	3.98E-04	3.58E-04	3.23E-04
H_2O	9.73E-02	2.01E-01	0	9.75E-02	2.02E-01
H_2SO_4	0	0	0	0	1.00E-07
N_2	7.62E-01	7.09E-01	7.79E-01	7.07E-01	6.21E-01
NO	1.41E-05	1.36E-05	2.31E-05	2.07E-05	1.85E-05
NO_2	6.00E-07	5.00E-07	1.50E-06	1.30E-06	1.10E-06
O_2	8.03E-02	7.98E-02	2.11E-01	1.87E-01	1.69E-01
SO_2	2.10E-06	2.10E-06	1.39E-03	1.28E-04	1.18E-04
SO_3	1.50E-06	1.50E-06	1.62E-04	1.40E-04	1.24E-04
Ar	0	0	8.93E-03	8.13E-03	7.42E-03

Figure 3. Cumulative probability of metal loss exceedance plots exposures in combustion atmospheres of 300 ppm SO_x in air containing 0, 10 and 20% H_2O at 700 °C in 80/20 (Na/K)$_2$SO$_4$ deposit applied cyclically with a flux of 1.5 µg/cm²/h.
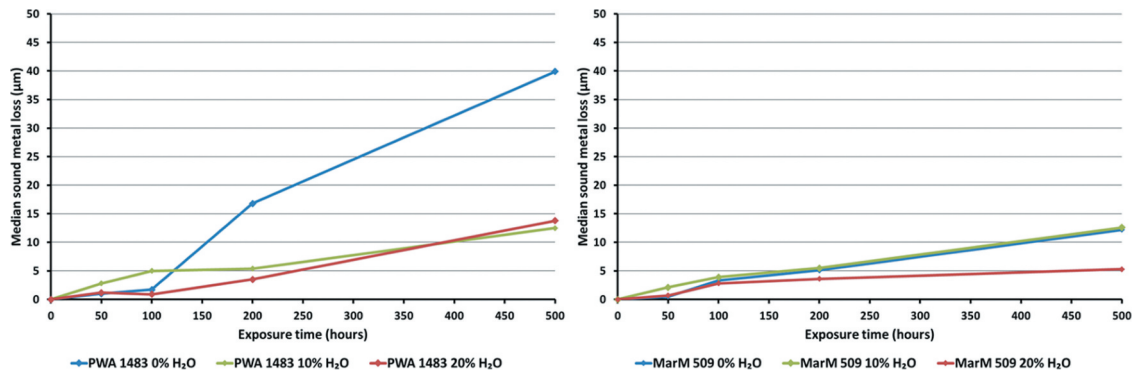
Figure 4. Median probability of metal loss exceedance plots exposures in combustion atmospheres of 300 ppm SO_x in air containing 0, 10 and 20% H_2O at 700 °C in 80/20 $(Na/K)_2SO_4$ deposit applied cyclically with a flux of 1.5 µg/cm^2/h.

The materials selection for this study included both a nickel-based superalloy, PWA 1483, and a cobalt-based superalloy, MarM 509. Both these alloys form a protective chromia scale and feature solid solution strengthening refractory metal carbide phases within the alloy matrix. The nominal compositions of these materials are given in Table 1. The area percentage of the alloy matrix that is made up of refractory metal carbides has been determined using Image J software [15], this was 0.9% for PWA 1483, and 6.2% for MarM 509. Samples were cylindrical in geometry with a chamfer machined at the top and bottom of the sample. The diameter and height were approximately 10 mm. Pre-test metrology of the sample dimensions was carried out using a digital micrometre with a resolution of ±1 µm.
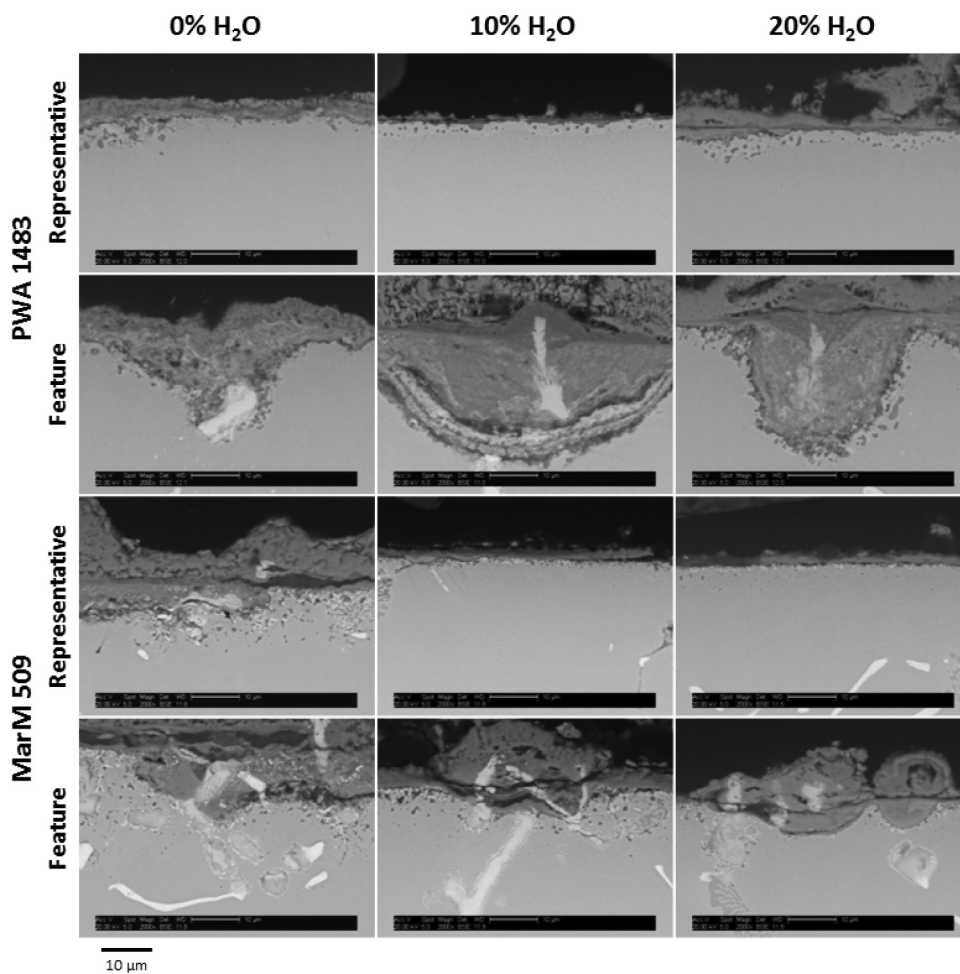

Figure 5. BSE micrographs of PWA 1483 and MarM 509 showing representative damage and corrosion features after 500 hours of exposure in 300 ppm SO_x in air containing 0, 10 and 20% H_2O at 700 °C with a 80/20 $(Na/K)_2SO_4$ deposit at a flux of 1.5 µg/cm^2/h.
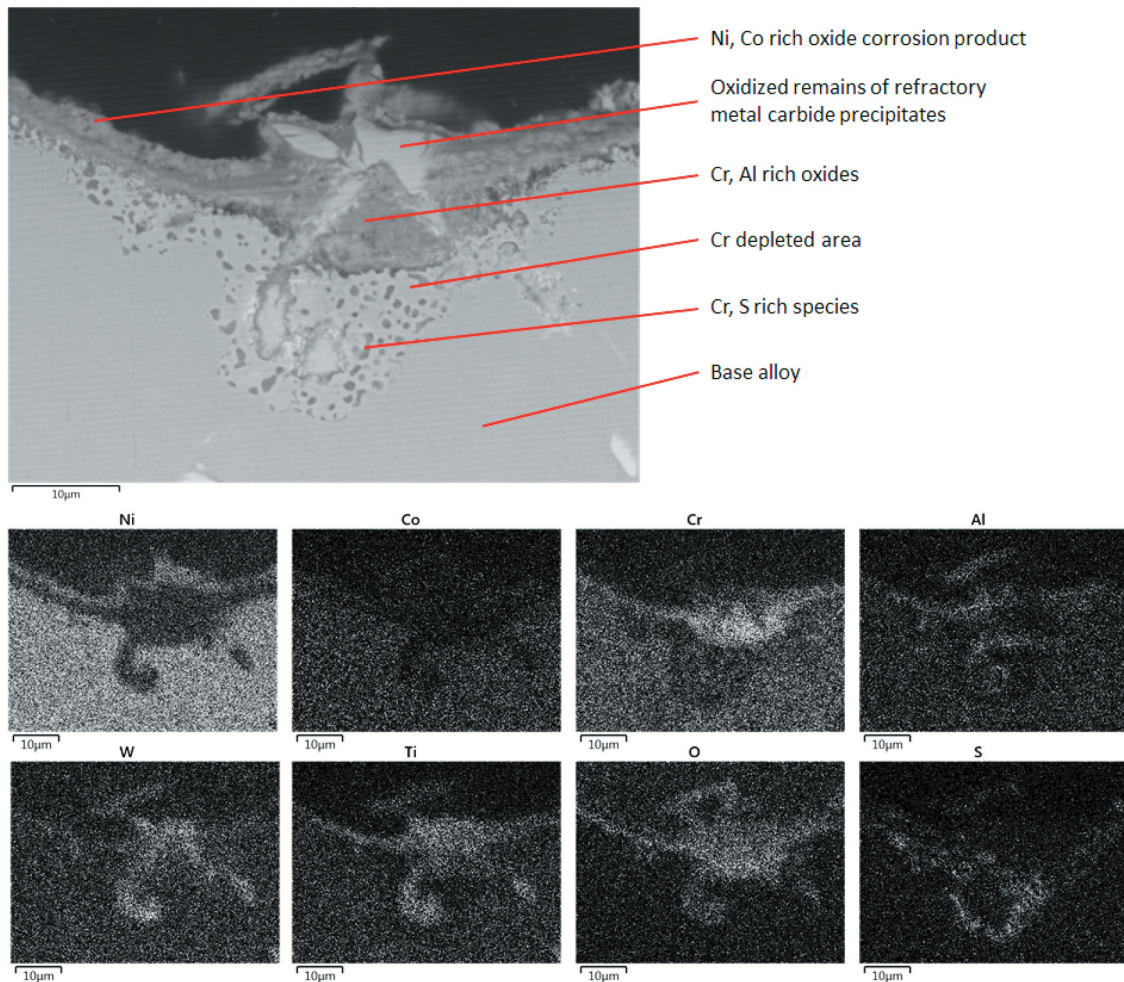
Figure 6. BSE image and associated EDX element maps of a corrosion feature on PWA 1483 after 500 hours of exposure at 700 °C in air containing 0 % H_2O at 700 °C with a 80/20 $(Na/K)_2SO_4$ deposit at a flux of 1.5 μg/cm^2/h.

ost test samples were mounted in a mixture of low shrinkage resin and ballotini (glass beads with a diameter of 0.04 to 0.07 mm. Samples were cross-sectioned, then ground and polished to a 1 μm finish using oil-based lubricants to avoid dissolving soluble species at the surface of the sample. Sample cross sections were measured at 30 points using an optical microscope with a calibrated x and y stage. Comparison with the pre-test metrology provided quantitative corrosion data. Qualitative assessment of corrosion morphology was carried out using an environmental scanning electron microscope (ESEM) outfitted with an energy dispersive X-ray (EDX) analysis system.

The partial pressure of species present in the different test atmospheres at 700 °C were determined using MT Data (NPL, UK) thermodynamic modelling software and are presented in Table 2. Of these species, SO_3 is particularly significant since it is known to stabilise the molten salt deposit [11]. In the 300 ppm SO_2 test atmospheres, the lower SO_3 partial pressures in the atmospheres containing H_2O can mostly be attributed to the dilution of the test gas with H_2O.

Results and discussion

Cumulative probability of change in sound metal exceedance plots are shown in Figure 3 for exposures containing 0, 10 and 20% H_2O respectively. The change in sound metal is defined as the metal lost from the metal surface plus any internal damage.

Both PWA 1483 and MarM 509 generally show a lesser change in sound metal as the concentration of H_2O in the atmosphere increases from 0% to 20%; this trend is more clearly illustrated in Figure 4. This finding runs counter to previous research (summarised in Figure 1) that observed an increasing change in sound metal with increasing water vapour. The mechanism behind this causing these contrasting trends is not clear; however, the key difference between these two studies lies in the SO_2 content in the test atmosphere (3.6 ppm in the previous research compared to 300 ppm) and any explanation for the difference in data trend is therefore likely based on atmospheric SO_x content. It is possible that where SO_x levels are in the order of 3.6 ppm, then oxidation becomes more important than fluxing mechanisms. When SO_x levels are in the order of 300 ppm, fluxing becomes the more
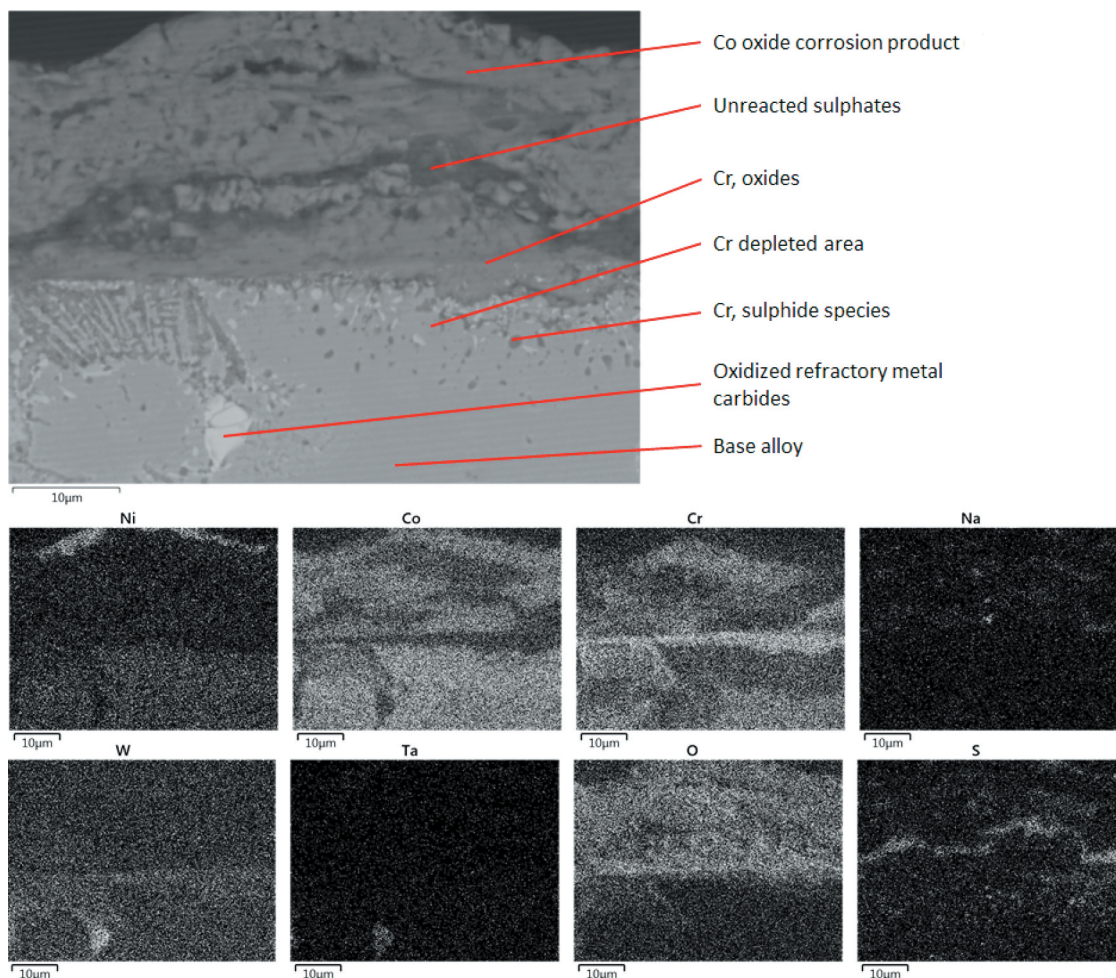
Figure 7. BSE image and associated EDX element maps of a corrosion feature on MarM 509 after 500 hours of exposure at 700 °C in air containing 0 % H_2O at 700 °C with a 80/20 $(Na/K)_2SO_4$ deposit at a flux of 1.5 μg/cm²/h.

dominant mechanism of degradation. Water vapour may exacerbate oxidation (as supported by the majority of the literature) but retard hot corrosion. This could be through interactions with the gas phase or with the molten deposit phase.

Compared to MarM 509, PWA 1483 suffers a greater degree of sound metal loss in exposures with the three tested levels of water vapour 0, 10 and 20%. This finding is in contrast to the previous research that observed MarM 509 suffering greater sound metal loss than PWA 1483 (Figure 1). SO_x in the gas phase is thought to shift the amphoteric behaviour of molten Na_2SO_4 towards being more acidic. One possible explanation for the contrasting data trends is that in atmospheres containing lower SO_x levels, alloy induced fluxing mechanisms brought about by refractory metal carbide precipitates in the alloy matrix become more important. MarM 509 has a greater proportion of such precipitates (6.2%) than PWA 1483 (0.9%) and therefore exhibits greater sound metal loss at a lower level of SO_x. At higher levels of SO_x other factors such as chromium content of the material may

become more important, of which MarM 509 has 27.1 at.% compared to 13.7 at.% for PWA 1483, to form a better protective scale.

If the logic holds true that at high temperatures, increasing levels of water vapour causes increasing levels of degradation of the chromia scale through volatisation, and that the better the chromia scale, the better an alloys type II hot corrosion resistance, then for increasing levels of water vapour to not increase the degree of type II hot corrosion attack, an additional mechanism must take place. Such a mechanism could involve the removal of corrosive species from the system thereby changing the acidity/basicity of the melt.

Backscattered electron (BSE) images both representative of the majority of the sample and corrosion features for PWA 1483 and MarM 509 after 500 hours of exposure at all tested levels of H_2O are shown in Figure 5. Most corrosion features of both PWA 1483 and MarM 509 exhibit internal damage which are shown to be species rich in both chromium and sulphur (Figures 6 and 7). The formation of chromium sulphide beneath the alloy surface is associated

with type I hot corrosion basic fluxing which is more commonly observed at temperatures between 850°C and 950°C [16]. The corrosion features in Figure 5 show that damage is not evenly distributed and has formed pits, while the corrosion product has formed an outer layer shown in Figure 5 to be rich in nickel and cobalt and an inner layer rich in chromium. These features are commonly associated with type II and the temperature range of 605°C to 750°C [16]. Features associated with type I and II hot corrosion occurring together can be termed mixed mode corrosion and support Rapp's fluxing mechanism [11] (later expanded upon by Gleeson [17]) whereby the acidity and basicity of the corrosion melt changes over time. Mixed mode corrosion features are seen to occur under conditions both with and without water vapour, therefore the presence of water vapour may not be connected to this phenomenon.

Micrographs representative of the majority of the samples' surfaces all exhibit at least some evidence of the formation of sulphide species beneath the alloy surface. These species are more numerous and have penetrated deeper in PWA 1483 compared to MarM 509.

For both PWA 1483 and MarM 509, corrosion pits have often, but not exclusively, formed around the oxidised remains of refractory metal carbide precipitates at the surface of the alloy. Such precipitates may exacerbate the hot corrosion process either by locally disrupting the formation of a continuous oxide scale or by allowing an alloy induced fluxing mechanism to occur [18,19].

Further research to thermodynamically model the phases that form under type II hot corrosion conditions that contain water vapour may shed light on the reason why water vapour appears to reduce the severity of type II hot corrosion attack and why only if the SO_x levels are sufficiently high. Additionally, further empirical data could reveal if the same phenomenon occurs under type I hot corrosion conditions (typically around 900 °C).

Conclusions

A series of laboratory type II hot corrosion tests investigated the effects of increasing atmospheric water vapour levels. Tests were carried out at 700 °C in an atmosphere of 300 ppm SO_2 in air with 0, 10 and 20% water vapour contents, and a 80% Na_2SO_4 20% K_2SO_4 deposit with a flux of 1.5 µg/cm^2/h.

Lower metal loss values were observed with increasing levels of water vapour in the test atmosphere. After 500 hours of exposure at water vapour levels of 0, 10 and 20% vol. respectively, the median metal loss values

of PWA 1483 were as follows: 39.9 µm, 12.5 µm and 13.8 µm. For MarM 509 the median metal loss values were as follows: 12.2 µm, 12.6 µm and 5.3 µm.

The hot corrosion performance of MarM 509 is better than PWA 1483 in the 300 ppm SO_2 test atmosphere at all three tested levels of water vapour. This is the opposite of the observations made in the previous research that had a test atmosphere containing 3.6 ppm SO_2, and 20% vol. H_2O). It is proposed that at lower levels of SO_2 in the environment, alloy induced fluxing mechanisms of refractory metal phases (of which MarM 509 has more than PWA 1483) become more important than gas-phase fluxing mechanisms.

Mixed mode hot corrosion features (features typical of both type I and II hot corrosion) were observed under all test conditions. Mixed mode hot corrosion features are thought to come about by changes in the deposit melt chemistry that can alter which fluxing mechanism is dominant.

Disclosure statement

ORCID

Andrew Potter http://orcid.org/0000-0003-3438-8966
Joy Sumner http://orcid.org/0000-0001-5435-200X
Nigel Simms http://orcid.org/0000-0002-8865-9138

References

[1] Oskarsson H. Material Challenges in Industrial Gas Turbines. Journal of Iron and Steel Research International. 2007;14(5):11–14

[2] Sumner J, Potter A, Simms NJ, et al. Hot corrosion resistance of gas turbine materials in combusted syngas environments. Mater. High Temp. 2015;32(1–2):177–187

[3] Poullikkas A. An overview of current and future sustainable gas turbine technologies. Renewable Sustainable Energy Rev. 2005;9(5):409–443.

[4] Sumner J, Potter A, Simms NJ, et al. Modeling gas turbine materials' hot corrosion degradation in combustion environments from H_2-rich syngas. Mater. Corros. 2017;68(2):205–214

[5] Saunders SRJ, Monteiro M, Rizzo F. The oxidation behaviour of metals and alloys at high temperatures in atmospheres containing water vapour: a review. Prog Mater Sci. 2008;53(5):775–837.

[6] Ehlers J, Young DJ, Smaardijk EJ, et al. Enhanced oxidation of the 9%Cr steel P91 in water vapour containing environments. Corros Sci. 2006;48(11):3428–3454.

[7] Asteman H, Svensson JE, Johansson LG. Evidence for chromium evaporation influencing the oxidation of 304L: the effect of temperature and flow rate. Oxid Met. 2002;57(3–4):193–216.

[8] Onal K, Maris-Sida MC, Meier GH, et al. "The Effects of Water Vapor on the Oxidation of Nickel-Base Superalloys and Coatings at Temperatures from 700°C to 1100°C," Superalloys 2004 (Tenth Int. Symp. 2004;5:607–615.

[9] Zurek J, Young DJ, Essuman E, et al. Quadakkers "Growth and adherence of chromia based surface scales on Ni-base alloys in high- and low-pO_2 gases. Mater Sci Eng. 2008;477(1–2):259–270.

[10] Pettit F. Hot Corrosion of Metals and Alloys. Oxid Met. 2011;76(1–2):1–21.

[11] Rapp RA. Hot corrosion of materials: a fluxing mechanism? Corros Sci. 2002;44(2):209–221.

[12] Giggins CS, Pettit FS. Hot corrosion degradation of metals and alloys - A unified theory. East Hartford: Pratt & Whitney Aircraft Group; 1979.

[13] Potter A, Sumner J, Simms NJ, et al., "Hot corrosion in the next generation of industrial gas turbines," vol. Conference. Eurocorr 2014. Pisa, 2014.

[14] Sumner S, Aksoul J, Delgado Q, et al. Impact of Deposit Recoat Cycle Length on Hot Corrosion of CMSX-4. Oxid Met. 2017;87(5–6):767–778.

[15] Potter A, Sumner J, Simms NJ. The role of superalloy precipitates on the early stages of oxidation and type II hot corrosion. Mater. High Temp. 2018;3409:1–7.

[16] Birks N, Meier GH, Pettit FS. Introduction to the high-temperature oxidation of metals. Vol. 2. Cambridge: Cambridge University Press; 2006.

[17] Alvarado-Orozco JM, Garcia-Herrera JE, Gleeson B, et al. Reinterpretation of Type II Hot Corrosion of Co-Base. Oxid Met. 2018;90(5):527–553.

[18] Lutz BS, Meier GH, Garcia-Fresnillo L. Na_2SO_4-Deposit-Induced Corrosion of Mo-Containing Alloys. Oxid Met. 2017;88(5):599–620.

[19] Potter A, Sumner J, Simms NJ. The role of superalloy precipitates on the early stages of oxidation and type II hot corrosion. Mater. High Temp. 2018;35(1–3):236–242